11th World Congress on Computational Mechanics (WCCM XI)
5th European Conference on Computational Mechanics (ECCM V)
6th European Conference on Computational Fluid Dynamics (ECFD VI)
E. Oñate, J. Oliver and A. Huerta (Eds)

NUMERICAL ANALYSIS OF RFSSW JOINTS

A. DERLATKA, K. KUDŁA, K. MAKLES

Czestochowa University of Technology
Dąbrowskiego 69, 42-201 Częstochowa, Poland
e-mail: aderlatka@bud.pcz.czest.pl

Key Words: *Finite element method, aluminium, Refill Friction Spot Stir Welding (RFSSW).*

Abstract. The paper presents numerical analysis of a tensile test for welded specimens made of 7075 T6 aluminum alloy. The specimens were joined by Refill Friction Spot Stir Welding (RFSSW). RFSSW is a method for joining metals in a solid state. The numerical calculations were performed using the ADINA System based on the Finite Element Method (FEM). Three different FE analyses were carried out for each specimen. In the first analysis, the sheets and joints were modeled with 3D elements. In the second analysis, the sheets and joints were modeled with shell elements. In the third analysis, the sheets were modeled with shell elements while the joints were modeled with 3D elements. The stress distributions were analyzed.

INTRODUCTION

Friction stir welding (FSW) is a solid-state joining technology that has recently received considerable attention from the aerospace and automotive industry. Refill friction stir spot welding (RFSSW) is a more recent application of the FSW process. RFSSW is an attractive process for manufacturers who need to reduce the weight of their assemblies by joining light-weight metals. Many kinds of aluminum alloys (2XXX and 7XXX alloyed series), which are generally considered as non-weldable, are successfully joined by the FSW technique [1]. A rotating tool (with a probe, sleeve, clamping ring) is used to create the joint. RFSSW joints are produced in two ways. In the first way, the probe is plunged into the workpieces, but the sleeve is retracted. At the same time, the welded material is transferred to the sleeve location. Upon reaching the desired plunge depth, the tool is kept in that position for a specified time. After that, the rotating tool is retracted from the welded joint and the material is pressed into the welded point. In the second method of producing RFSSW joints, the sleeve is plunged into the workpieces, but the probe is retracted as shown in Fig. 1. The use of RFFSW leads to reduced cycle times, greater joint strength, and lower manufacturing costs [2]. Papers [3, 4] present influence of the process parameters.

According to [5, 6], engineering the design of structures requires numerical models which are capable of accurately describing the complete local mechanical behavior at large plastic strains. Several techniques are used for modeling RFFSW joins. One of the methods uses shell elements for modeling both the weld zone and base metal. The approach relies on performing a large deformation analysis and updating the thickness of the shell elements iteratively during the incremental solution. This method requires relatively small incremental steps and is only attractive when the strains throughout the shell thickness are not very large. Shell structures

are now solved in practice using 4-node shell elements.

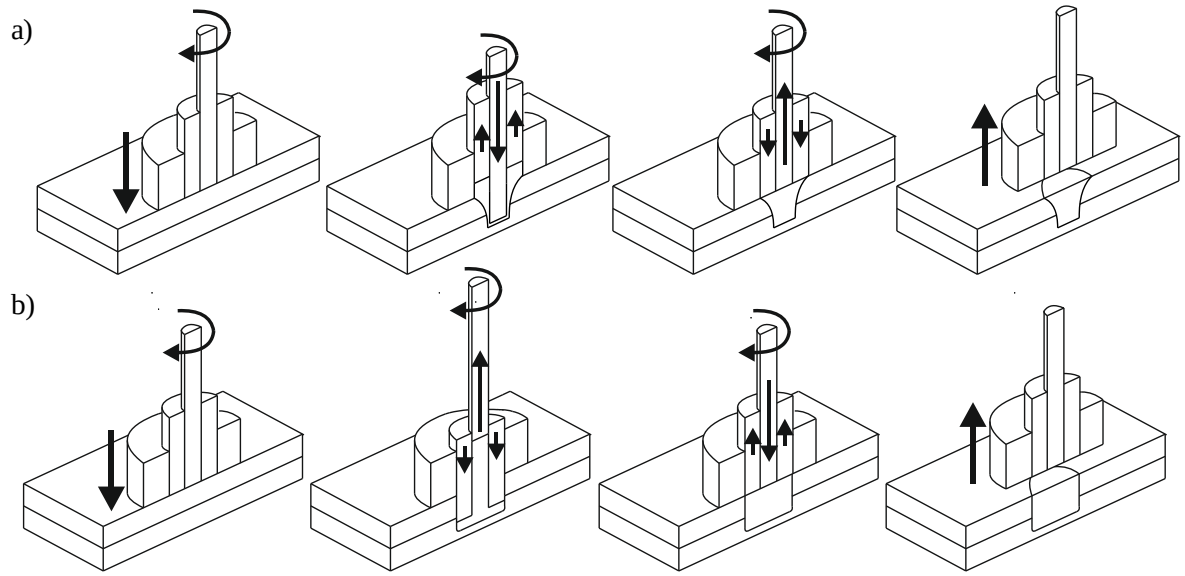

Figure 1: Schematic illustration of RFSSW process variants: a) plunged probe, b) plunged internal bushing

The second method is modeled by using three-dimensional (3D) solid elements. Typically 12-node or 27-node elements are used. There is a high computational cost associated with that method. Very finite meshes may need to be used and large strain shell problems can be complicated to solve [7].

The third approach uses the three-dimensional continuum theory to develop 3D-shell elements. These elements contain the kinematics of the three-dimensional solid elements used in the second approach, however, the geometry and displacement behavior are described with variables on the shell midsurface only. For example, the 12-node solid element reduces to a 4-node shell element and the 27-node solid element reduces to a 9-node shell element. The modeling and computational times are shorter compared to full three-dimensional analysis, especially if many different configurations have to be analyzed during the initial design phase of a structure. In [8 - 11], good agreement of the results from shell/3D simulations and full solid models are demonstrated.

GOAL AND SCOPE OF WORK

The choice of the numeric model for determining the tensile strength of RFSSW joints is the goal of this paper. Sheets of 7075 aluminium alloy are welded as lap joints.

Three types of geometry with different arrangement of the joints are analysed – Fig. 2. Three types of model are compared for each geometry:

- full 3D model for joints and sheets,
- shell elements for joints and sheets,
- shell elements for sheets and 3D elements for joints.

The effective stresses are analised in the numerical study.

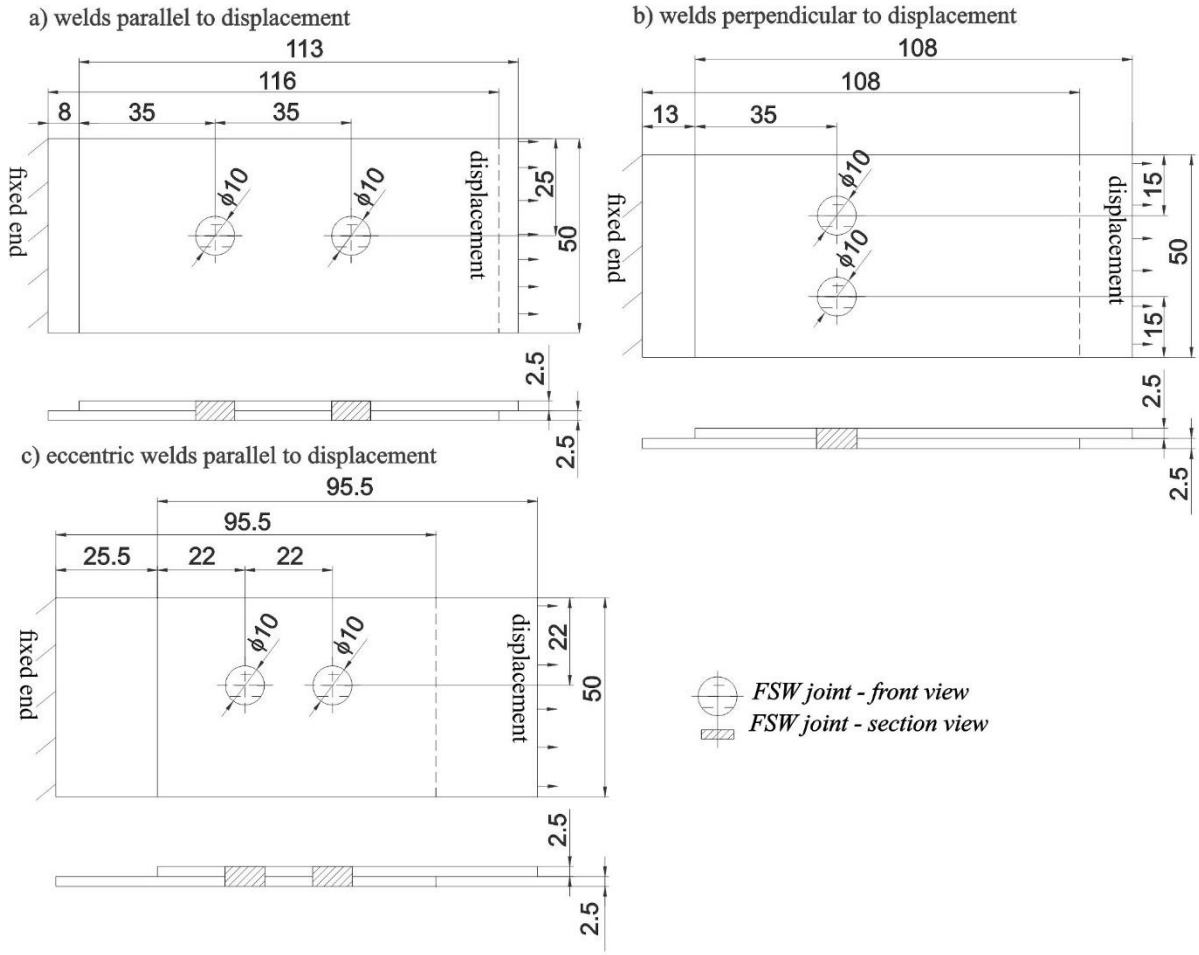

Figure 2: Geometry of the analyzed samples

COMPUTATIONAL MODELS

The numerical studies were carried out with the ADINA System based on the Finite Element Method. The boundary conditions and type of load are the same for each sample: all the degrees of freedom on the first external edge of the sample are fixed, the second external edge of the sample has one free degree of freedom (X-translation) and that edge is loaded by displacement. Plastic orthotropic material is used for each model. The following material parameters are defined for each direction: modulus of elasticity 69.61 GPa, yield strength 269 MPa, Poisson's ratio 0.33 and density 2810 kg/m3. That material model is used by the ADINA requirements because of the simultaneous application of finite elements, like shell and 3D.

In the first model, the sheets and joints are modeled as 8-node 3D elements. Between the 3D element surfaces of the sheets, the contact conditions are assumed. The boundary conditions and load are then added to the surfaces. In the second model, the sheets and joints are modeled as 4-node shell elements. Between the sheet elements, the contact conditions are assumed. Between the shell elements of the joints, rigid links are assumed and then the contact conditions are assumed. The boundary conditions and load are afterwards added to the lines. In the third model, the sheets are meshed as 4-node shell elements, but the joints are meshed as 8-node 3D

elements. Between the shell elements the contact conditions are assumed. The boundary conditions and load are then added to the lines.

Table 1 presents the number of nodes and finite elements in each joint model.

Table 1: Numer of nodes and finite elements

		number of shell finite elements	number of volume finite elements	number of nodes
joints parallel to displacement	sheets - shell, joints - 3D	5760	6144	13304
	sheets - shell, joints - shell	6784	-	6946
	sheets - 3D, joints - 3D	-	37136	34112
joints perpendicular to displacement	sheets - shell, joints - 3D	4000	3200	8188
	sheets - shell, joints - shell	4400	-	4558
	sheets - 3D, joints - 3D	-	17600	22548
eccentic we joints lds parallel to displacement	sheets - shell, joints - 3D	3224	2400	6424
	sheets - shell, joints - shell	3624	-	3762
	sheets - 3D, joints - 3D	-	14496	18568

In each model, the sheet and joint elements are connected in nodes. The details of the connections are shown in Fig. 3.

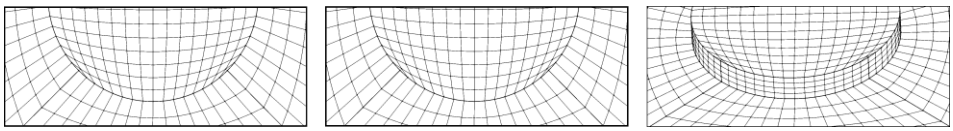

Figure 3: The detail of connections: a) 3D elements, b) shell elements, c) 3D element with shell element

RESULTS

The effective stresses for a sample with parallel joints modeled as 3D elements for sheets and joints, for the sample with joints and sheets modeled as shell elements and for the sample with sheets modeled as shell elements and joints modeled as 3D are presented in Figures 4, 5 and 6 respectively.

The effective stresses for a sample with perpendicular joints modeled as 3D elements for sheets and joints, for the sample with joints and sheets modeled as shell elements and for the sample with sheets modeled as shell elements and joints modeled as 3D are presented in the Figures 7, 8 and 9.

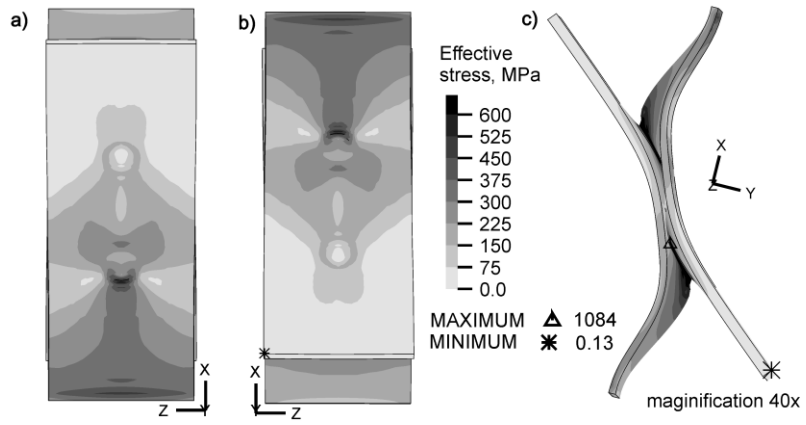

Figure 4: Effective stresses for sample with parallel joints with sheets and joints modeled as full-3D, a) front view, b) bottom view, c) axonometric view, MPa

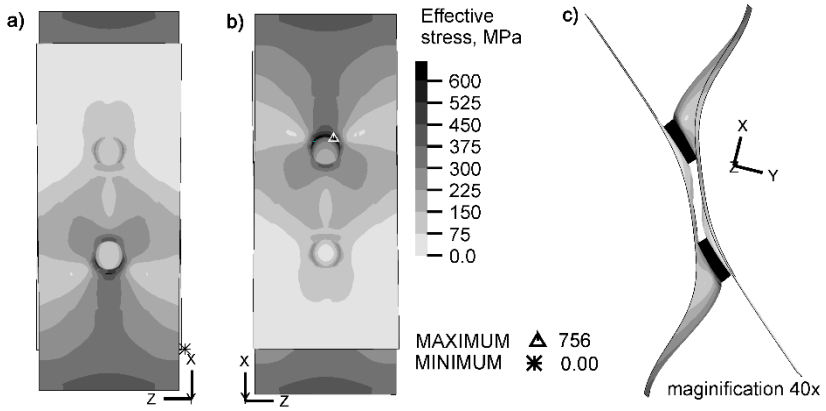

Figure 5: Effective stresses for sample with parallel joints with sheets and joints modeled as shell elements, a) front view, b) bottom view, c) axonometric view, MPa

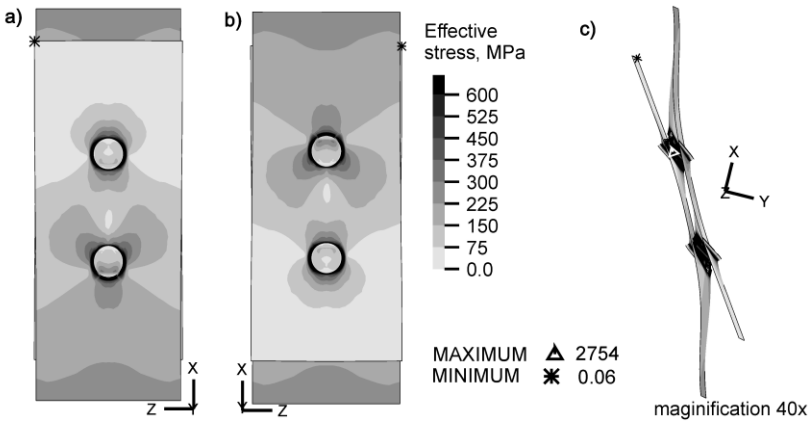

Figure 6: Effective stresses for sample with parallel joints with sheets modeled as shell elements and joints modeled as 3D, a) front view, b) bottom view, c) axonometric view, MPa

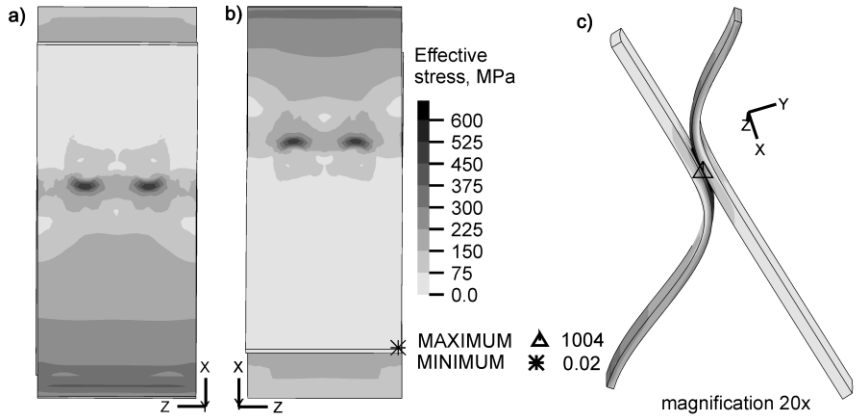

Figure 7: Effective stresses for sample with perpendicular joints with sheets and joints modeled as 3D elements, a) front view, b) bottom view, c) axonometric view, MPa

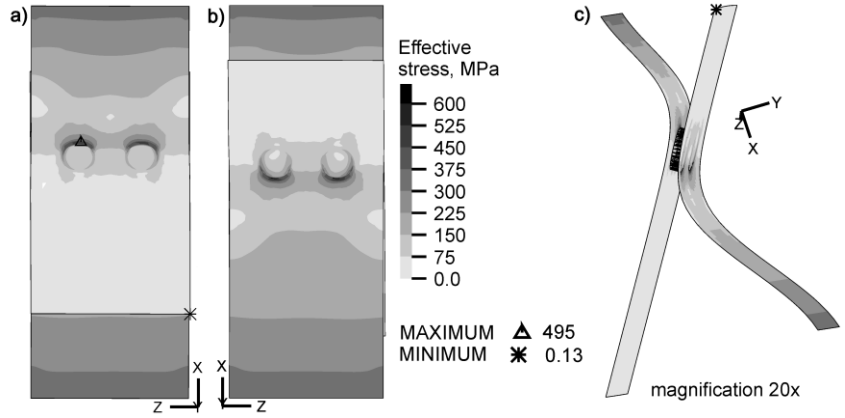

Figure 8: Effective stresses for sample with perpendicular joints with sheets and joints modeled as shell elements, a) front view, b) bottom view, c) axonometric view, MPa

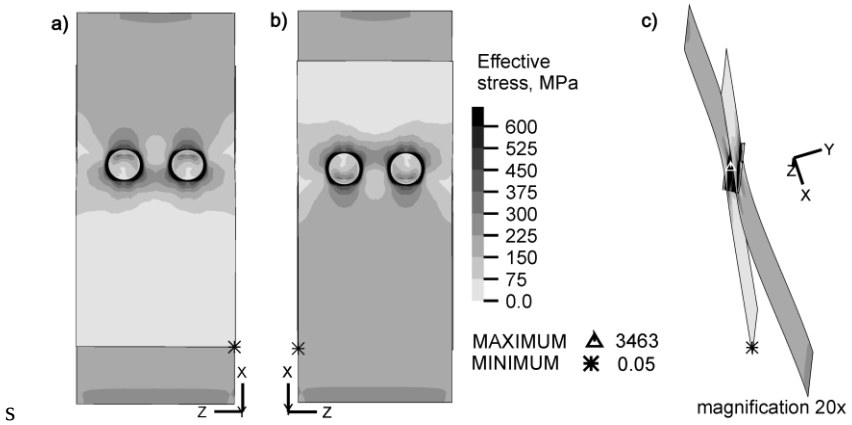

Figure 9: Effective stresses for sample with perpendicular joints with sheets modeled as shell elements and joints modeled as full-3D, a) front view, b) bottom view, c) axonometric view, MPa

The effective extreme stresses are presented in the above Figures. For each sample, regardless of the method of modeling, the stresses distribution is symmetrical with respect

to the X-axis and similar in both sheets. In each sample, with the same joint arrangement, the stresses distribution is comparable, the maximum is concentrated on the outer edge of the joints, the minimum is on the free edge of the sheet. Based on the analysis of the stresses in the joints, the lowest stresses are concentrated in the center of each joint.

The effective stresses for the sample with eccentric parallel joints with joints and sheets modeled as 3D elements, for the sample with joints and sheets modeled as shell elements and for the sample with joints modeled as 3D and sheets modeled as shell elements are presented in Figures 10, 11 and 12 respectively.

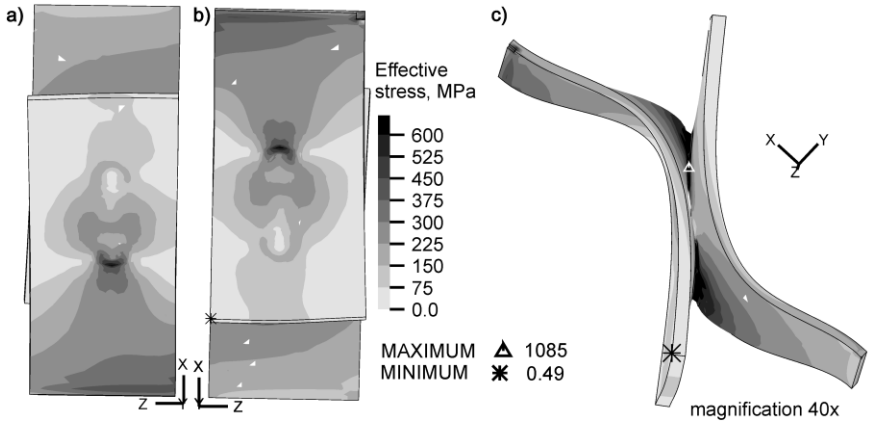

Figure 10: Effective stresses for sample with eccentric parallel joints with sheets and joints modeled as 3D elements, a) front view, b) bottom view, c) axonometric view, MPa

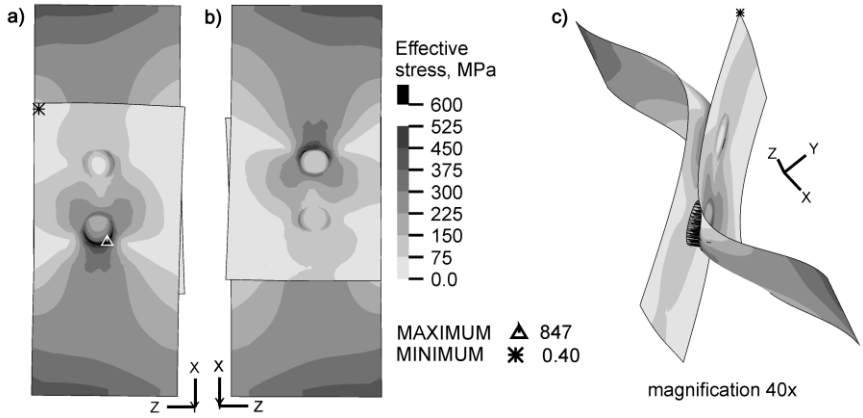

Figure 11: Effective stresses for sample with eccentric parallel joints with sheets and joints modeled as shell elements, a) front view, b) bottom view, c) axonometric view, MPa

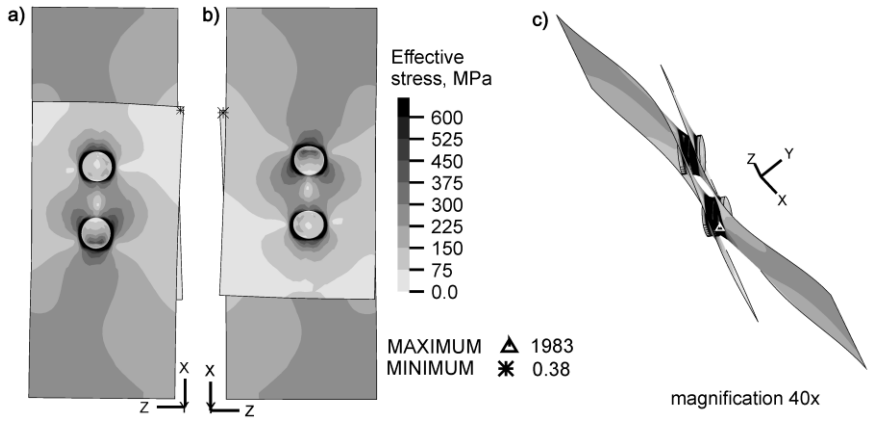

Figure 12: Effective stresses for sample with eccentric parallel joints with sheets modeled as shell elements and joints modeled as full-3D, a) front view, b) bottom view, c) axonometric view, MPa

The effective extreme stresses for the sample with eccentric parallel joints are presented in the Figures above. For each model, the stress distribution is not symmetrical with respect to the x-axis and different in both sheets. In each model, regardless of the method of modeling, the stresses distribution is comparable, the maximum is concentrated on the outer edge of the joints, the minimum is on the free edge of the sheet. According to the analysis of the stresses in the joints, the lowest stresses are concentrated in the center of each joint .

Table 2 presents the total solution time and the total memory used by the program in each joint model.

Table 2: Total solution time and total memory used by the program

kind of joint	model	total solution time [s]	total memory used by the program [mb]
joints parallel to displacement	sheets - shell, joints - 3D	338.74	303.7
	sheets - shell, joints - shell	228	161.4
	sheets - 3D, joints - 3D	1907.26	938.8
joints perpendicular to displacement	sheets - shell, joints - 3D	209.95	162.5
	sheets - shell, joints - shell	117.06	100.9
	sheets - 3D, joints - 3D	814.83	543.0
eccentic joints parallel to displacement	sheets - shell, joints - 3D	150.73	124.7
	sheets - shell, joints - shell	89.46	79.9
	sheets - 3D, joints - 3D	642.71	426.6

DISCUSSION

In Table 3, the percentage comparison of the total solution time and total memory used by the program are presented. The differences of the extreme results for three models with the same joint arrangements are caused by using different kinds of finite elements. Every kind of finite element is characterized by another way of averaging the results. The full 3D model is about 7-8 times longer and it needs about 5 times more total memory than the full shell model. The model with sheets modeled as shell elements and joints modeled as 3D elements is about 1.5 - 4 times longer and it needs about 1.5 - 3 times more total memory than the full shell model.

Table 3: Percent comparison of total solution time and total memory used by the program

kind of joint	model comparison	percent of total solution time, %	percent of total memory used by the program, %
joints parallel to displacement	sheets - 3D, joints - 3D vs sheets - shell, joints - shell	837	582
	sheets - shell, joints - 3D vs sheets - shell, joints - shell	149	309
joints perpendicular to displacement	sheets - 3D, joints - 3D vs sheets - shell, joints - shell	696	538
	sheets - shell, joints - 3D vs sheets - shell, joints - shell	388	334
eccentic joints parallel to displacement	sheets - 3D, joints - 3D vs sheets - shell, joints - shell	718	534
	sheets - shell, joints - 3D vs sheets - shell, joints - shell	426	156

The 3D finite elements are the most exact, but they need more computational time than the shell elements, which are less accurate. The full shell model or model with 3D and sell elements could be used for preliminary calculations, to determine the weakest area in the structure. For accurate analysis of structure the full 3D is more recommended. However, the full 3D model might be used only for small constructions, due to the restrictions: long total solution time and significant requirements of computers. For large structures, only simplified models might be used.

The location of effective extreme stresses in RFSSW joints, namely the maximum on the edges of joints and minimum in the center of joints is a consequence of the circular shape of the joints. Torsion is a reason for the asymmetrical stresses distribution in the sample with eccentric parallel joints.

CONCLUSIONS

The analysis of RFSSW joints with a different arrangement of joints and different method for modeling are investigated. The following conclusions are made:

- It is possible to model those joints in three ways: RFSSW joints and sheets modeled as 3D elements, RFSSW joints and sheets modeled as shell elements, RFSSW joints modeled as 3D elements and sheets modeled as shell elements.

- The most accurate way for modeling is by using 3D elements for the whole model while the quickest way for modeling is by using shell elements for the whole model.
- In the each sample, the concentration of effective stresses is observed on the outer edge of the joints.
- The effective stresses in the RFSSW joints are higher than in the raw material.

ACKNOWLEDGMENT

Financial support of Structural Funds in the Operational Programme - Innovative Economy (IE OP) financed from the European Regional Development Fund - Project "Modern material technologies in aerospace industry", Nr POIG.01.01.02-00-015/08-00 is gratefully acknowledged.

REFERENCES

[1] P. Lacki, A. Derlatka, *The application of FSW technology in aluminium structures,* Metal forming (2013) 24: 205-218.

[2] B.T. Gibson, D.H. Lammlein, T.J. Prater, W.R. Longhurst, C.D. Cox, M.C. Ballun,K.J. Dharmaraj, G.E. Cook, A.M. Strauss, *Friction stir welding: Process, automation, and control,* Journal of Manufacturing Processes (2014) 16: 56–73.

[3] Lacki P., Wojsyk K, Kudła K., Śliwa R.E, *Friction welding of the bars made of aluminium and titanium alloys,* European Congress on Computational Methods in Applied Sciences and Engineering (2012): 5029-5041.

[4] Lacki P., Kucharczyk Z., Śliwa R.E, Gałaczyński T., *Effect of tool shape on temperature field in friction stir spot welding,* Archives of metallurgy and materials (2013) 58: 595-599.

[5] T. Sussman, K.J. Bathe, *3D-shell elements for structures in large strains,* Computers and Structures (2013) 122: 2–12.

[6] D.N. Kim, K.J. Bathe, *A 4-node 3D-shell element to model shell surface tractions and incompressible behavior,* Computers and Structures (2008) 86: 2027–2041.

[7] S. Tutunchilar, M. Haghpanahi, M.K. Besharati Givi, P. Asadi, P. Bahemmat, *Simulation of material flow in friction stir processing of a cast Al–Si alloy,* Materials and Design (2012) 40: 415–426.

[8] R. Krueger, P.J. Minguet, *Analysis of composite skin–stiffener debond specimens using a shell/3D modeling technique,* Composite Structures (2007) 81: 41–59.

[9] R. Krueger, T.K. O'Brien, *A shell/3D modeling technique for the analysis of delaminated composite laminates,* Composites: Part A (2001) 32: 25–44.

[10] R. Krueger, J.G. Ratcliffe, P.J. Minguet, *Panel stiffener debonding analysis using a shell/3D modeling technique,* Composites Science and Technology (2009) 69: 2352–2362.

[11] P. Fanelli, F. Vivio, V. Vullo, *Experimental and numerical characterization of Friction Stir Spot Welded joints,* Engineering Fracture Mechanics (2012) 81: 17-25.